PECULIARITIES OF SINGLE-SIDED CW LASER BEAM IMAGING OF SMALL-DEPTH INHOMOGENEITIES IN HIGHLY-SCATTERING MEDIA

T. DREISCHUH, L. GURDEV, O. VANKOV, E. TONCHEVA, L. AVRAMOV, D. STOYANOV

Institute of Electronics, Bulgarian Academy of Sciences
72 Tzarigradsko Chaussee, Sofia 1784, Bulgaria
Email: *tanjad@ie.bas.bg*

Compiled August 24, 2018

In this paper, we report some seemingly extraordinary features found experimentally and interpreted theoretically of images derived by optical sensing of small-depth characteristic inhomogeneities (inclusions, e.g., ill places in tissues) in homogeneous highly-scattering host media (e.g., healthy tissues), such as dilutions of Intralipid-20% emulsion in distilled water. It is shown experimentally that at a relatively small depth of the inhomogeneities, when they are not yet enveloped entirely by the scattering-widened laser beam, one may observe an inverted or/and double image of an inclusion, depending on the host-medium turbidity and on the inhomogeneity-to-host medium contrast. The effects observed result from some features of the intensity distribution of laser light backscattered from homogeneous liquid tissue-like phantoms of different turbidity. The results obtained would help one to develop optical (cw laser-beam assisted) diagnostics and tomography approaches and to solve the so-called specificity problem by unambiguous interpretation of the captured tissue images.

Key words: Optical tomography, tissue optics, tissue-mimicking phantoms, Intralipid optical properties.

1. INTRODUCTION

The methods for single-sided optical sensing and diagnostics of tissues and other highly scattering media, based on continuous-wave (cw) laser irradiation of the investigated objects and direct detection of the backscattered light [1], have not been so popular so far compared for instance to the coherent [2, 3] or pulsed time-to-range resolved direct detection [4] such approaches. They may be more advantageous however in a sense than the other above-mentioned approaches because, e.g., they would not require special high-repetition-rate short-pulse laser transmitters neither extremely fast signal-recording electronics nor sophisticated delicately-adjustable interferometric devices. Therefore, it is worth estimating theoretically and experimentally their imaging and diagnostics potentialities [5, 6]. The single-sided detection and imaging in this case of characteristic inhomogeneities (inclusions, e.g., ill places in tissues) in highly-scattering homogeneous host media (e.g., healthy tissues) is performed by evaluating the difference between the backscattered-light intensity distri-

butions over the entrance/exit plane of the medium in the presence and absence of inclusions. According to the conventional wisdom, the information-carrying signal (image) obtained in such a way should be positive and stronger at a higher turbidity of the inclusion compared to that of the host medium; and vice versa, in the opposite case. This is the case when the inhomogeneity of interest is located at a relatively large depth in the host medium, say, above 1 cm in front of the sensing laser beam. An image inversion or/and doubting effect is observable however at smaller depths of the inclusions. Then, the "positive" inclusions (ingredients) may produce "negative" (inverted) and even double-peak images, and vice versa. Such an effect is interesting in itself and important for deciphering the characteristics of the corresponding inclusions. Therefore, the main purpose of the present work is to study this effect in detail experimentally, to explain its peculiarities in a semiquantitative theoretical way, and to estimate its applied potential.

2. EXPERIMENTAL ARRANGEMENT, APPROACH AND MATERIALS

The experimental arrangement employed in this work is sketched in Fig. 1 (see also in [5]). It is intended for measuring the backscattered-light intensity distribution over a "frontal" entrance/exit plane of a turbid medium irradiated normally by a stationary cw laser beam. The experiments are performed with a homogeneous highly-scattering host medium containing or not characteristic contrasting inhomogeneities. An image of the inclusions is obtainable as the difference between the intensity distributions obtained with and without them. The tissue-mimicking phantoms under investigation consist as a whole of a plexiglass $12 \times 12 \times 22\,\mathrm{cm}$ parallelepiped-form container filled with liquid turbid media. The container is irradiated by a collimated laser diode-emitted beam of wavelength $\lambda = 847\,\mathrm{nm}$, power ($P_\mathrm{L} = \pi A^2 I_0$) about $20\,\mathrm{mW}$ and radius $A = 1.5\,\mathrm{mm}$; I_0 is the initial on-axis intensity of the laser beam.

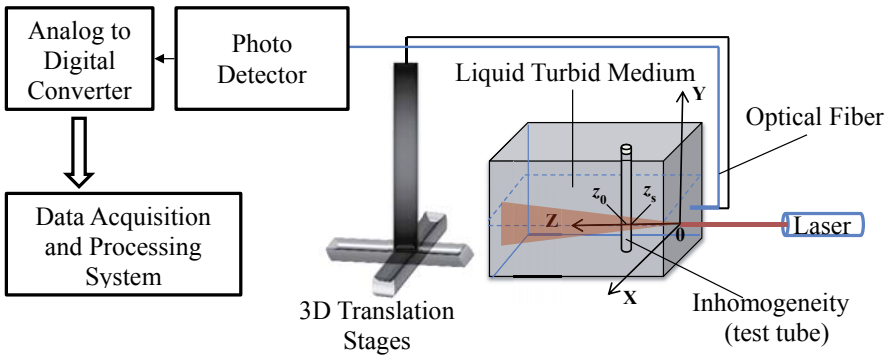

Fig. 1 – Experimental setup

The axis of the beam determines an axis $0z$ with initial point $0(0,0,0)$ lying on the internal frontal wall. Two additional horizontal, $0x$, and vertical, $0y$, axes lying on the same wall complete along with $0z$ a right coordinate system given in Fig. 1.

The liquid turbid media employed in the work are dilutions in distilled water of different concentrations of Intralipid-20% (Fresenius Kabi AB, Sweden) emulsions. Intralipid (IL) is a fat emulsion, made up of soybean oil, egg yolk phospholipids, glycerin, and water, that is widely used in optical experiments to simulate the scattering properties of biological tissues [7–9]. The main reason for that is the low absorption coefficient at visible and near-infrared wavelengths and the possibility to adjust the scattering coefficient by changing the concentration of the solutions. The Intralipid concentration has usually been considered as the volume fraction of soybean oil and egg lecithin forming the submicron pellets in the dilution [7]. This volume fraction in Intralipid-20% is 22.74%.

The inhomogeneities in the host media are made again of Intralipid-20% dilutions in distilled water infused into test tubes of glass that may have different internal diameters. Certainly, the inhomogeneity concentration is different from that of the host medium. The test tubes are introduced into the host medium perpendicular to the plane $\{0xz\}$ and can be translated in depth and laterally. In the experiments of interest here, a test tube of diameter $d = 10\,\mathrm{mm}$ is mainly employed, disposed in front of the laser beam at different (varied) depths along axis $0z$. The backscattered light power distribution $J(\vec{\rho})$ ($\vec{\rho} = \{x, y\}$) over the external frontal wall of the container is measured by using a scanning optical fiber of $0.1\,\mathrm{mm}$ core diameter with an additional accessory to narrow the angle of acceptance γ to $\sim 0.01\,\mathrm{rad}$. The receiver aperture radius E is about $0.45\,\mathrm{mm}$. The fiber is oriented parallel to the beam axis and is connected with an optical radiometer Rk-5100 (Laser Precision Corp., USA) in external locking regime, with a RqP-546 silicon probe, 14 bits analog-to-digital converter and a computer for appropriate data processing. The noise equivalent power (NEP) of the radiometer is $2 \times 10^{-12}\,\mathrm{W}$. Its averaging (low-pass filtering) time constant is chosen to be 1 s. To avoid a disturbance of the laser beam the transversal distribution of the detected power $J(\vec{\rho})$ is measured by scanning the fiber parallelly to axis $0x$, but at some fixed minimum distance ($y = y_\mathrm{c} = const$) from it. The fiber scan is realized by using a linear translation stage with an integrated stepper motor and controller LTS 300/M (Thorlabs, Inc., USA) ensuring a minimum sampling step of $4\,\mu\mathrm{m}$. The measured shape $J(\vec{\rho})$ describes in fact the intensity distribution of the backscattered light because the receiver aperture radius and angle of acceptance are much smaller respectively than the transversal and angular variation scales of the backscattered light radiance over plane $z = 0$.

The image of an inhomogeneity in a host medium is obtainable in principle as the difference $J_\mathrm{d}(x, y_\mathrm{c}) = J_1(x, y_\mathrm{c}) - J_2(x, y_\mathrm{c})$ between the intensity distributions J_1 and J_2 obtained respectively in the presence and the absence of the inhomogeneity.

In practice, the distribution $J_2(x, y_c)$ is measured with the test tube present again (in the corresponding place) but filled with the material of the host medium. Thus, a compensation is achieved for the tube glass (1.2 mm thick) influence on the image formation. Such a compensation leads to results near those obtainable in the case of no tube. Just this case is interpreted theoretically below. So far as the experiments are performed in a dark laboratory at practically entirely removed stray light influence, and NEP of the radiometer is negligible compared to the least measured powers of interest, the signal fluctuations should mainly be due to the signal-conditioned shot noise [10], the digitizing noise, the laser power fluctuations, and the scintillations due to the random walk of the particles within the scattering volume. By using in the experiments a low-pass filtering with $1\,\mathrm{s}$ time constant along with 400 measurements per point, the relative root-mean-square (rms) signal fluctuations are reduced to a level of about 1%. Note as well that the error in the determination of J_d should be about twice larger than the error in the determination of J_1 or J_2. Then, an inhomogeneity will be recognizable when J_d exceeds essentially the summary level of fluctuations of J_1 and J_2.

3. EXPERIMENTAL RESULTS, SEMIQUANTITATIVE THEORETICAL ANALYSIS AND DISCUSSION

The Intralipid concentrations C_h of the host media used in the experiments occupy a large interval from 0.2% to 3%. The concentrations C_i of the inhomogeneities considered vary within the same interval. The shapes of the inhomogeneity images for different pairs (C_h, C_i) have been measured and analysed, depending on the inhomogeneity depth in the host medium. This depth will be specified by coordinates z_s and/or z_0 along axis $0z$ that are, respectively, the frontal intercept of the test tube with axis $0z$ and the intercept of the test tube axis with axis $0z$. Here, we shall illustrate and semiquantitatively interpret the image metamorphosis in depth for some typical combinations (C_h, C_i).

Let us first consider the case when both the IL concentrations C_h and C_i exceed 0.7%. The image evolution observed experimentally in this case is illustrated in Fig. 2 for two concentration pairs - $C_\mathrm{h} = 1.73\%$ and $C_\mathrm{i} = 2.84\%$ (top row), and $C_\mathrm{h} = 2.793\%$ and $C_\mathrm{i} = 1.749\%$ (bottom row). It is seen in the figure that when the inhomogeneity is near the entrance wall of the container, at depths $z_0 = 6.2\,\mathrm{mm}$ or $7.2\,\mathrm{mm}$ ($z_s = 0\,\mathrm{mm}$ or $1\,\mathrm{mm}$, respectively), instead of the conventionally expected "positive" image in the upper row and "negative" one in the lower row, we have an inverted picture. That is, the images in the upper row are negative, and in the lower row are positive. With increasing the depth along the laser beam axis, the (negative or positive) peaks of the images decrease and pass through a "zero position" (where a noise is mainly measured) around $z_s = 2\,\mathrm{mm}$. Further, they are inverted and acquire

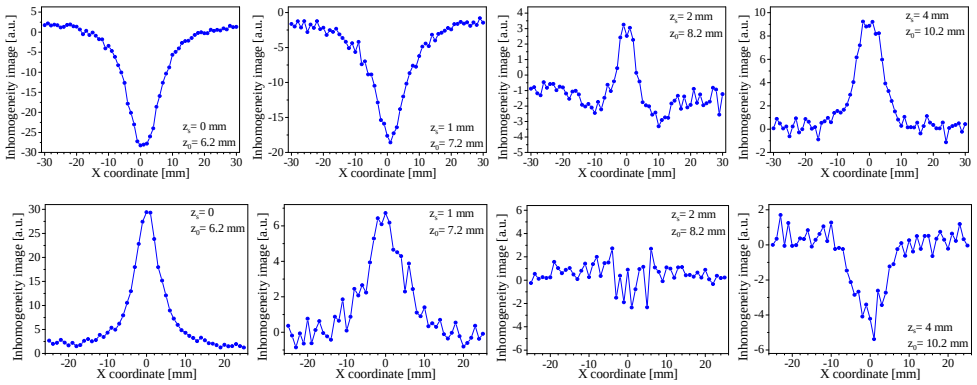

Fig. 2 – Inhomogeneity images obtained at Intralipid concentrations of 1.73% and 2.84% (top row) and 2.793% and 1.749% (bottom row) of the host medium and inhomogeneity, respectively, and different depths $z_0(z_s)$ of the test tube along the line of sight $0z$.

their "true sign" corresponding to the (positive or negative) inhomogeneity contrast with respect to the host medium. The peaks of the "true" images first increase with z to some value of $z_s \sim 4-5\,\mathrm{mm}$. Then, they begin to diminish with z as it is observed formerly in [5]. Such a behavior of the images, especially at small inhomogeneity depths, can be explained on the basis of the results obtained in [6], where the entrance/exit - plane intensity distribution is studied experimentally and theoretically of the backscattered light from homogeneous turbid media irradiated by a collimated (Gaussian on the average) cw laser beam. It is supposed that the scattering function of the considered turbid media is of Henyey-Greenstein type [11] and is shown that the theoretical and experimental results obtained are consistent for values of the anisotropy factor $g \sim 0.8 \div 0.85$. It is shown as well [6] that the intensity distribution along a line transversal to the laser beam (e.g., $||0x$) and at some distance (say $y_\mathrm{c} = 8\,\mathrm{mm}$) from its axis has a bell-shaped form with a peak at $x = 0$. At relatively small IL concentrations $C \lesssim 0.7\%$, the peak values increase with C, reaching a maximum around $C = 0.7\%$. The further increase of C leads to decreasing the peak values. The contour of the intensity distribution, $J(x, y_\mathrm{c})$, also changes with C so that its near-bottom, wing area is narrowed. The described evolution with C of the intensity distribution peak and contour is due to strong widening and increased attenuation of the laser light beam within the turbid medium. With increasing C, the depth of formation D_f of the backward light flux decreases along with the width of the backscattering layers of concern. The depth D_f can be estimated conditionally, on the basis of the theoretical expression (at $g = 0.85$) of the measurable intensity distribution (see Appendix A), as

$$D_\mathrm{f} \sim 1.556\,\mathrm{MFP}_\mathrm{tr}\,, \tag{1}$$

where $\mathrm{MFP_{tr}} = \mu_{\mathrm{sr}}^{-1}$ is the transport mean free path of the photon in the turbid medium, $\mu_{\mathrm{sr}} = \mu_{\mathrm{s}}(1-g)$ is its reduced-scattering coefficient, and μ_{s} and g are the corresponding integral scattering coefficient and anisotropy factor (see, e.g., in [12]). The e^{-1}, e^{-2}, e^{-3} and e^{-4} radii of a backscattering layer of the medium at a depth z are estimated to be (Appendix A)

$$R_{\mathrm{e}n}(z) \sim (0.35nz^3/\mathrm{MFP_{tr}})^{1/2} \,, \tag{2}$$

where n = 1,2,3, and 4, respectively. Then, the corresponding wing - area width conditioning layer radii $R_{\mathrm{we}n}$, at a depth $z = D_{\mathrm{f}}$ and $g = 0.85$, will be

$$R_{\mathrm{we}n} = R_{\mathrm{e}n}(z = D_{\mathrm{f}}) \sim Q_n \mathrm{MFP_{tr}} \,, \tag{3}$$

with Q_n = 1.15, 1.62, 1.99, and 2.30. Obviously, the values of $R_{\mathrm{we}n}$ are inversely proportional to the medium turbidity, that is, to μ_{s}. The values of $\mu_{\mathrm{s}}(C) \sim \mu_{\mathrm{e}}(C)$, as a function of the IL concentration C, are determined on the basis of experimental data obtained in [13] for the corresponding (to $\lambda = 847\,\mathrm{nm}$) extinction coefficient $\mu_{\mathrm{e}}(C)$ whose best-fit quadratic dependence (in cm^{-1}) is

$$\mu_{\mathrm{e}}(C) = 2.01 + 14.89C - 0.54C^2 \,. \tag{4}$$

Let us further note that the e^{-1} width $w_{\mathrm{b}}(z)$ of an initially collimated Gaussian laser light beam, at a depth z in a turbid medium, is estimated in [14] to be

$$w_{\mathrm{b}}(z) = [(1+g)z^3/18\,\mathrm{MFP_{tr}}]^{1/2} \tag{5}$$

provided that the medium scattering function is of Henyey-Greenstein type.

When a test tube containing a contrasting inhomogeneity is touching or very near the entrance wall into the parallelepiped box, the laser light beam there is still too narrow compared to the contrasting area. So, it hits directly this area and when the Intralipid concentration inside, C_{i}, is sufficiently high, the backward light flux will be formed in practice entirely within the test tube. Then, if C_{h} and $C_{\mathrm{i}} > 0.7\%$ IL, it is clear that a positive inhomogeneity $(C_{\mathrm{i}} > C_{\mathrm{h}})$ will provide a negative image and vice versa. With increasing the inhomogeneity depth $z_0(z_s)$, the contribution to the backward light signal of the host medium increases, and that of the inhomogeneity decreases. So, a depth is reached, where the peak values of J_1 and J_2 are comparable. Then, there is no clear image, and noise is mainly measured. At a further increase of the depth, when the test tube is already entirely involved by the scattering - widened light beam in the box [when $2w_b(z) > d$], the backscattered light fluxes are formed mainly in the host medium with an additional (decreasing with depth) inhomogeneity contribution. In this case, a "normal-sign" image appears, corresponding to the inhomogeneitity sign, whose peak initially slightly increases and then decreases with z. The peak value is now proportional to the inhomogeneity contrast and inversely proportional to the depth. The transversal image size equals that of the inclusion. The

transition from an anomalius to normal image should take place around and above the depth

$$z_0 = z_t = [4.5\, d^2 \mathrm{MFP_{tr}}/(1+g)]^{1/3}\,, \tag{6}$$

according to Eq.(5) for $w_{\rm b}(z = z_t) = d/2$. For $g = 0.85$ we have

$$z_t = (2.43\, d^2 \mathrm{MFP_{tr}})^{1/3}\,. \tag{7}$$

When $C_{\rm h} = 1.73\%\,\mathrm{IL}$ ($\mathrm{MFP_{tr}} \cong 2.55\,\mathrm{mm}$) and $C_{\rm i} = 2.84\%\,\mathrm{IL}$ ($\mathrm{MFP_{tr}} \cong 1.67\,\mathrm{mm}$), according to Eq.(7) we obtain that the anomalous-to-normal image transition takes place at depths z_0 around $z_t \sim 8.5\,\mathrm{mm}$. In this case, the depth of formation $D_{\rm f}$ [Eq.(1)] of the backward light flux in the inhomogeneity medium is $\sim 2.6\,\mathrm{mm}$ ($< d = 10\,\mathrm{mm}$). The radii $R_{\mathrm{we}n}$ in the host medium and inhomogeneity medium [Eq.(3)] have comparable values, respectively, $R_{\rm we1} = 2.92$ and $1.92\,\mathrm{mm}$, $R_{\rm we2} = 4.14$ and $2.71\,\mathrm{mm}$, $R_{\rm we3} = 5.07$ and $3.32\,\mathrm{mm}$, and $R_{\rm we4} = 5.86$ and $3.83\,\mathrm{mm}$. Thus, when the inhomogeneity is near the frontal wall ($z_s \to 0$) the backward light flux is formed entirely within the test tube, and the distribution $J_1(x, y_{\rm c})$ is as if obtained by scattering from an infinite homogeneous medium. Then, so far as $C_{\rm h}$ and $C_{\rm i}$ exceed $0.7\%\,\mathrm{IL}$ and the radii $R_{\mathrm{we}n}$ in both the media have comparable values, we obtain a negative bell-shaped initial image $J_{\rm d}(x, y_{\rm c})$ that is gradually transformed with the depth, around and above $z = z_t \sim 8.5\,\mathrm{mm}$, into a normal positive and informative image as it is seen in the top row of Fig. 2. Similar but inverted is the picture (Fig. 2, bottom row), when $C_{\rm h} = 2.793\%\,\mathrm{IL}$ ($\mathrm{MFP_{tr}} \approx 1.69\,\mathrm{mm}$) and $C_{\rm i} = 1.749\%\,\mathrm{IL}$ ($\mathrm{MFP_{tr}} \approx 2.52\,\mathrm{mm}$). In this case, $z_t \sim 7.44\,\mathrm{mm}$, $D_{\rm f} \sim 3.93\,\mathrm{mm}$, and the corresponding $R_{\mathrm{we}n}$ are: $R_{\rm we1} = 1.94$ and $2.90\,\mathrm{mm}$, $R_{\rm we2} = 2.45$ and $4.10\,\mathrm{mm}$, $R_{\rm we3} = 3.37$ and $5.02\,\mathrm{mm}$, and $R_{\rm we4} = 3.89$ and $5.80\,\mathrm{mm}$.

Consider further the case when both $C_{\rm h}$ and $C_{\rm i} < 0.7\%\,\mathrm{IL}$. In this case, the peak of the distribution $J(x, y_{\rm c})$ increases with increasing the concentration of the corresponding homogeneous scattering medium. At the same time, the wing area width decreases. When $C_{\rm h} = 0.205\%\,\mathrm{IL}$ ($\mathrm{MFP_{tr}} = 13.23\,\mathrm{mm}$) and $C_{\rm i} = 0.494\%\,\mathrm{IL}$ ($\mathrm{MFP_{tr}} = 7.22\,\mathrm{mm}$), we have $z_t \sim 14.76\,\mathrm{mm}$, $D_{\rm f} \sim 11.24\,\mathrm{mm}$, and, respectively $R_{\rm we1} = 15.19$ and $8.29\,\mathrm{mm}$, $R_{\rm we2} = 21.49$ and $11.73\,\mathrm{mm}$, $R_{\rm we3} = 26.32$ and $14.36\,\mathrm{mm}$, and $R_{\rm we4} = 30.39$ and $16.58\,\mathrm{mm}$. So, at $z_s \to 0$, the distribution $J_1(x, y_{\rm c})$ is formed mainly but not entirely within the test tube. Nevertheless, it should be narrower and higher than $J_2(x, y_{\rm c})$, which explains the initial image shape in Fig. 3, top row. As may be expected, the sign of this shape, including both lower side lobes, corresponds to the positive inhomogeneity contrast, and the "normal" inhomogeneity image is achieved around $z_0 \sim 10\,\mathrm{mm}$. The opposite case, when $C_{\rm h} = 0.505\%\,\mathrm{IL}$ ($\mathrm{MFP_{tr}} = 7.10\,\mathrm{mm}$) and $C_{\rm i} = 0.205\%\,\mathrm{IL}$ ($\mathrm{MFP_{tr}} = 13.23\,\mathrm{mm}$), is a little different. It is illustrated in Fig. 3, bottom row. In this case, $z_t \sim 12\,\mathrm{mm}$, $D_{\rm f} \sim 20.59\,\mathrm{mm}$, and $R_{\rm we1} = 8.16$ and $15.19\,\mathrm{mm}$, $R_{\rm we2} = 11.53$ and $21.49\,\mathrm{mm}$, $R_{\rm we3} = 14.12$ and $26.32\,\mathrm{mm}$, and $R_{\rm we4} = 16.31$ and $30.39\,\mathrm{mm}$. Thus, the backscattered light flux in

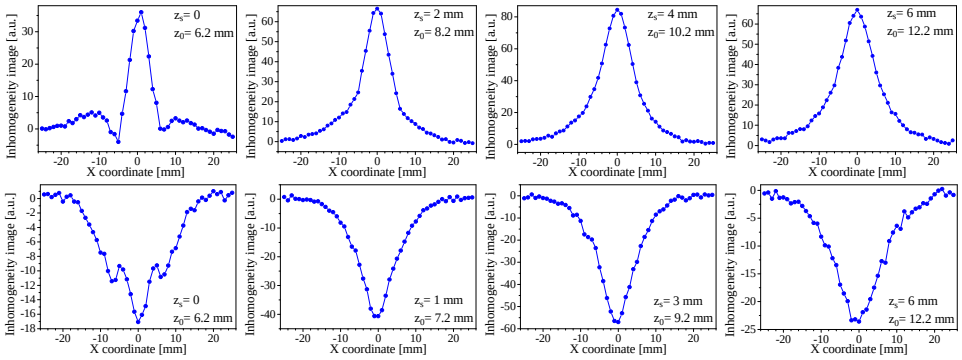

Fig. 3 – Same as in Fig. 2 but for Intralipid concentrations of 0.205% and 0.494% (top row) and 0.505% and 0.205% (bottom row) of the host medium and inhomogeneity, respectively.

the presence of inhomogeneity is formed not only within the test tube but in the host medium as well. Due to the host-medium influence, the small-depth image form is more complicated. Nevertheless, the sign of the image shape coincides again with that of the inhomogeneity contrast.

The effects observed, described and discussed above, are too complicated to be completely interpreted on the basis of an accurate detailed theory. Therefore, they are explained in a semiquantative way. In some cases, however, when the inhomogeneity has a high turbidity and the backward light flux is formed entirely inside it, the image obtained experimentally is explanable just as the difference of the "images" (backscattered light intensity distributions) of two homogeneous media, the inhomogeneity medium and the host medium. Such is the case when $C_{\rm h} = 0.406\%\,{\rm IL} < 0.7\%$ and $C_{\rm i} = 2.067\%\,{\rm IL} > 0.7\%$. The image evolution with depth in this case is illustrated in Fig. 4. Correspondingly, in Fig. 5 it is shown that the small-depth images observed experimentally are expressible as the difference between the above-mentioned "images". Let us note as well that the distribution $J(x, y_{\rm c})$ obtained from an infinite homogeneous medium of concentration $C = 0.406\%\,{\rm IL}$ is higher and wider compared to that obtained at $C = 2.067\%\,{\rm IL}$. When $C_{\rm h} = 0.406\%\,{\rm IL}$ $({\rm MFP_{tr}} = 8.37\,{\rm mm})$ and $C_{\rm i} = 2.067\%\,{\rm IL}$ $({\rm MFP_{tr}} = 2.19\,{\rm mm})$, we obtain that $z_t \sim 12.67\,{\rm mm}$, $D_{\rm f} \sim 3.40\,{\rm mm}$ and, respectively, $R_{\rm we1} = 9.61$ and $2.51\,{\rm mm}$, $R_{\rm we2} = 13.59$ and 3.55, $R_{\rm we3} = 16.68$ and $4.35\,{\rm mm}$, and $R_{\rm we4} = 19.22$ and $5.02\,{\rm mm}$. Thus, the distribution $J_2(x, y_{\rm c})$ conditioned by the host medium is much wider (~ 4 times) than that, $J_1(x, y_{\rm c})$, conditioned (in practice, entirely) by the inhomogeneity medium. As a result, the inverted double peak image $J_{\rm d}(x, y_{\rm c})$ in Fig. 4 is obtained at $z_s \to 0$. With increasing the depth z_0, around z_t $(\sim 12.67\,{\rm mm})$ and above, the role of the host medium in the formation of $J_1(x, y)$ increases. So, $J_2(x, y_{\rm c})$ (in the difference $J_{\rm d} = J_1 - J_2$) is gradually compensated with the depth z_0 and only

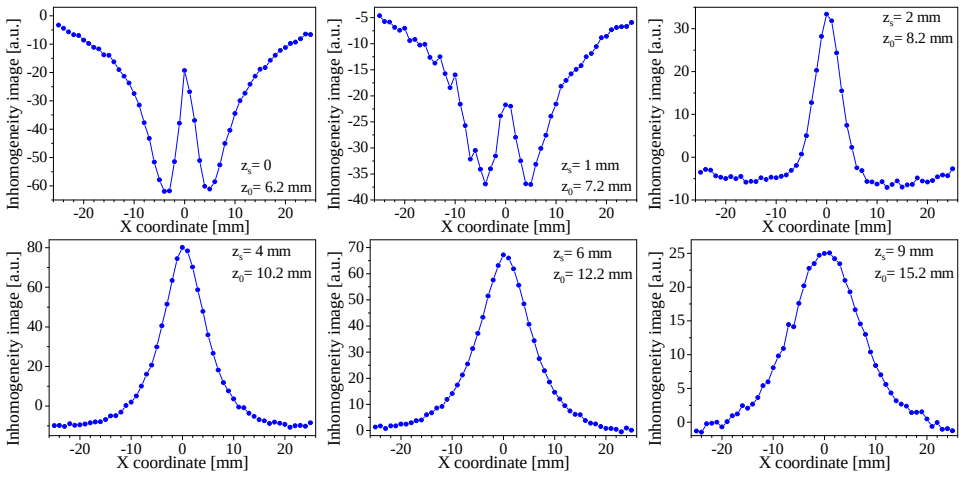

Fig. 4 – Same as in Fig. 2 but for IL concentrations $C_{\rm h} = 0.406\%$ and $C_{\rm i} = 2.067\%$.

the informative positive ("right sign") contrasting component of $J_1(x, y_{\rm c})$ remains. Experimentally determined distributions of concern here, $J_1(x, y_{\rm c})$, $J_2(x, y_{\rm c})$ and $J_{\rm d}(x, y_{\rm c})$, at $z_s = 0$, are compared in Fig. 5 with the corresponding theoretically suggested curves at $g = 0.865$. Both the groups of curves seem very similar to each other.

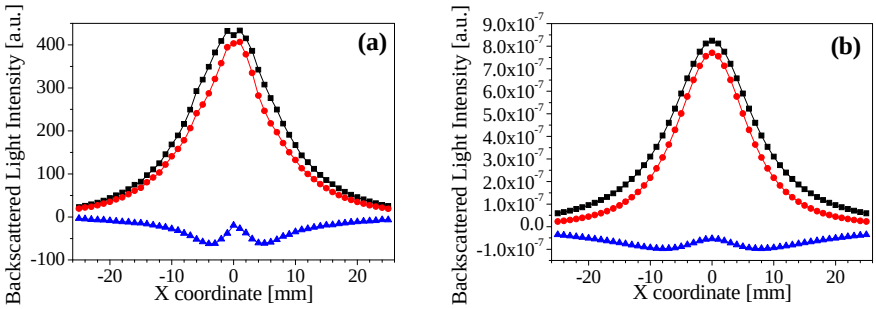

Fig. 5 – (a) Measured bacscatter power distributions from the investigated host medium ($C_{\rm h} = 0.406\%$ IL) with (red circles) and without (black squares) inhomogeneity ($C_{\rm i} = 2.067\%$ IL) and their difference (inhomogeneity image, blue triangles - see Fig. 4, $z_s = 0$). (b) Theoretical curves (and their difference, blue triangles) of $J(x, y_{\rm c})$ for $C = 2.067\%$ IL (red circles) and 0.406% IL (black squares) evaluated on the basis of Eq.(A.1) at $g = 0.865$.

As a whole, the analysis of the experimental results performed in this section shows that when $C_{\rm h}$ and $C_{\rm i} > 0.7\%$ IL, the small depth inhomogeneity images are inverted in sign with respect to the inhomogeneity-to-host medium contrast. When $C_{\rm h}$ and $C_{\rm i} < 0.7\%$ IL, the sign of the small-depth images coincide with that of the

inhomogeneity contrast. When $C_{\rm h} < 0.7\%\,{\rm IL}$ and $C_{\rm i} > 0.7\%\,{\rm IL}$, or vice versa, such images may have more complicated shapes, but with the following rule being in power. When the Intralipid dilution of higher concentration ($C_{\rm h}$ or $C_{\rm i}$) produces a lower-peak distribution $J(x, y_{\rm c})$, the small-depth image is inverted. In the opposite case, the image is not inverted. It is important to note that the $1D$ images under discussion here are not taken along the diameter of the laser beam cross section but along a chord at a distance $y_{\rm c}$ from the beam axis. At different values of $y_{\rm c}$ (other than 8 mm), one would obtain dividing concentration thresholds other than 0.7% and, in general, other types of images. In any case, all $1D$ images obtained should be fragments of the full $2D$ image that includes also the chords through the laser beam and its axis. Measuring $1D$ images through the laser beam is a serious experimental task whose solution is now in progress. A general conclusion from the above-conducted investigations is that the ($1D$ and $2D$) small-depth inhomogeneity images are specifically distorted depending on the inclusion type and respectively sign, shape and consistence. The images become undistorted only at depths z_0 exceeding z_t, where the inhomogeneity is covered entirely by the laser light beam in the host medium. A sufficiently detailed and accurate classification of the small-depth inclusion images would be of use for a contactless short-distance optical diagnostics of specific sections in tissues.

4. SUMMARY

In this work, an approach is investigated for single-sided, cw laser irradiation based detection of characteristic inhomogeneities (ill places) in highly scattering homogeneous host media (healthy tisues). The host media and inhomogeneities are prepared of dilutions of Intralipid-20% emulsion in distiled water. $1D$ inhomogeneity images are mainly investigated obtained as the difference between the backscattered-light intensity distributions, in the presence and absence of inclusions, along a line of scanning $0x$ lying on the entrance/exit plane of the host medium. The line of scanning is perpendicular to the laser beam and is at some distance y_c from its axis $0z$. It is also perpendicular to the inclusion that is a test tube of glass filled with a contrasting turbid medium. The test tube axis passes through the laser beam axis. A special attention is payed to the small-depth inhomogeneity images, when the inclusion is touching or near the frontal wall of the experimental container and the laser beam is still too narrow and not covering the inclusion. In this case, it is observed experimentally that, depending on the relation between the host-medium and inhomogeneity concentrations, the images may be inverted or not with respect to the inhomogeneity contrast sign and to have double-peak and even three-peak shape. The observed here peculiarities are explained on the basis of the theoretical and experimental results

obtained in [6], where it is shown that when $y_c \neq 0$, there exists a corresponding threshold concentration value $C = C_{th}$ such that the peak of the distribution $J(x, y_c)$ is increasing function of C, when $C < C_{th}$, and decreasing function, when $C > C_{th}$. The wing-area width of $J(x, y_c)$ is a decreasing function for all values of C. At a small inhomogeneity depth, the distribution $J_1(x, y_c)$ is formed entirely, mainly, or to a high extent, depending on C_i, within the test tube, and distribution $J_1(x, y_c)$ is near that, $J(x, y_c)$, obtained from an infinite turbid medium of concentration C_i. Then, the image is as if the difference of distributions $J(x, y_c)$ for concentrations C_i and C_h, respectively. This idea and the above-described peculiarities of the distributions $J(x, y_c)$ explain the peculiarities of the images of small-depth disposed inclusions. With increasing the depth of an inclusion, its image gradually changes and acquires a real image shape whose peak and transversal size correspond to the inhomogeneity contrast, depth and size. The transition from an anomalous to a real $1D$ or $2D$ image of an inclusion takes place around and above a depth $z = z_t$, where the inclusion is already entirely enveloped by the scattering-widened in the host medium laser beam. The specific small-depth inhomogeneity images can help the contactless short-distance optical diagnostics and recognition procedures of specific anomalies in tissues.

Acknowledgements. This work has been supported by the Bulgarian National Science Fund under the project DFNI-B02/9/2014 "Development of biophotonics methods as a basis of oncology theranostics".

A. ANALYTICAL EXPRESSION OF THE INTENSITY DISTRIBUTION $J(\vec{\rho})$

An analytical expression of the radial intensity distribution $J(\vec{\rho})$ of the backscattered light from a homogeneous turbid medium over the frontal wall of the medium irradiated by a collimated Gausian laser beam, is [6]

$$J(\vec{\rho}) = \beta \int_0^L d\eta \frac{\pi^2 A^2 I_0 E^2 \gamma^2}{[\eta^2\gamma^2 + E^2 + A^2 + \eta^2/(k^2A^2) + B^2(\eta)]} \times \exp\{-2\eta\mu_{te} - \rho^2/[\eta^2\gamma^2 + E^2 + A^2 + \eta^2/(k^2A^2) + B^2(\eta)]\} \ , \tag{A.1}$$

where

$$\beta = \mu_{sr}/[4\pi(1+g)^2], \tag{A.2a}$$

$$\mu_{te} = \mu_a + (\mu_{sr}/2g)[(1+g)/\sqrt{1+g^2} - 1] \ , \tag{A.2b}$$

and

$$B^2(\omega) = \mu_{sr}\omega^3[(1+g)/(9g^3)] \times [(1+g^2)^{3/2} - (1-g)^3 - 3g(1-g) - (3/2)g^2/\sqrt{1+g^2}] \ ; \tag{A.2c}$$

$k = 2\pi/\lambda$. At $g = 0.85$, we obtain that $0.75(2\mu_{\rm te})^{-1} \sim 1.556{\rm MFP}_{\rm tr}$. This quantity is conditionally assumed to be the depth of formation, D_f, of the backward light flux. At this depth in the turbid medium (at $\eta = D_{\rm f}$), the integrand peak in Eq.(A.1) (at $\vec{\rho} = \vec{0}$) diminishes $\sim \exp(0.75)[1 + 0.35D_{\rm f}^3/({\rm MFP}_{\rm tr}A^2)]$ times, or for instance ~ 10 times for Intralipid concentrations C = 2.84% and 2.793%, 20 times for C = 1.73% and 1.749%, 140-150 times for C = 0.494% and 0.505%, and 490 times for C = 0.205%, which corresponds to about 90%, 95%, 99.3%, and 99.8% - formed backward light flux. Note as well that in Eq.(A.1), the quantity $\eta^2(\gamma^2 + k^{-2}A^{-2}) + E^2$ is negligible with respect to $A^2 + B^2(\eta)$. The e^{-n} radii R_{en} of a scattering layer at a depth $\eta = z$ are estimated as

$$R_{en} \sim [nB^2(z)]^{1/2} \, . \tag{A.3}$$

Then, the corresponding estimates of the wing-area outlining radii $R_{{\rm w}en}$ are obtained from (A.3) for $z = D_{\rm f}$. That is,

$$R_{{\rm w}en} \sim [nB^2(D_{\rm f})]^{1/2} \, . \tag{A.4}$$

When $g = 0.85$, the estimates (A.3) and (A.4) lead to relations (2) and (3).

REFERENCES

1. M. Patachia, S. Banita, C. Popa, and D. C. Dumitras, Rom. Rep. Phys. **67**, 412–422 (2015).
2. W. Drexler and J.G. Fujimoto, *Optical Coherence Tomography: Technology and Applications*, Springer, Berlin, 2008.
3. A.G. Pehoiu, I. Popescu, C. Giurcaneanu, A.M. Forsea, Rom. Rep. Phys., in press (2018).
4. L. Gurdev, T. Dreischuh, and D. Stoyanov, Proc. SPIE **6604**, 66042I (2007).
5. L. Gurdev, T. Dreischuh, O. Vankov, E. Toncheva, L. Avramov, and D. Stoyanov, Bulg. J. Phys. **43**, 215–223 (2016).
6. L. Gurdev, T. Dreischuh, O. Vankov, E. Toncheva, L. Avramov, and D. Stoyanov, Proc. SPIE **10226**, 102261B (2017).
7. H. J. van Staveren, C. J. Moes, J. van Marie, S. A. Prahl, and M. J. C. van Gemert, Appl. Opt. **30**, 4507–4514 (1991).
8. S. T. Flock, S. L. Jacques, B. C. Wilson, W. M. Star, and M. J. C. van Gemert, Lasers Surg. Med. **12**, 510–519 (1992).
9. R. Michels, F. Foschum, and A. Kienle, Opt. Express **16**, 5907–5925 (2008).
10. R. M. Measures, *Laser Remote Sensing*, Wiley, New York, 1984.
11. A. Ishimaru, *Wave Propagation and Scattering in Random Media*, Vol. 1. Academic Press, New York, 1978.
12. F. Martelli, S. Del Bianco, A. Ismaelli, G. Zaccanti, *Light propagation through biological tissue and other diffuse media: Theory, Solutions, and Software*, SPIE Press, Bellingham, Washington, 2010.
13. L. Gurdev, T. Dreischuh, O. Vankov, D. Stoyanov, L. Avramov, J. Mod. Opt. **64**, 1270–1282 (2017).
14. L. Gurdev, T. Dreischuh, O. Vankov, I. Bliznakova, L. Avramov, and D. Stoyanov, Appl. Phys. B **115**, 427–441 (2014).